Supporting Information for

"Numerical analysis of time-dependent conduit magma flow in dome-forming eruptions with application to Mount St. Helens 2004-2008"

Ying-Qi Wong [1] **, and Paul Segall** [1]

[1]Department of Geophysics, Stanford University, Stanford, CA, USA

Contents

S1 Derivation of momentum balance

In the conduit model, magma flow in the viscous regime is simulated as Poiseuille Flow: laminar, fully-developed, steady and incompressible. In this section, we derive and justify the momentum balance equation via a scaling analysis of the Navier-Stokes equation for flow through a cylindrical pipe.

S1.1 Reynolds number, Mach number, entrance length ratio and conduit radius-to-length ratio

We present four non-dimensional quantities relevant to the scaling analysis. First, the Reynolds number determines if flow is laminar or turbulent. The Reynolds number

---

Corresponding author: Ying-Qi Wong, yqwong@stanford.edu

depends on density, cross-sectional area, velocity and viscosity. Density of typical magmas are $\sim 10^3$ kg/m^3. For the Mount St. Helens 2004-2008 dome-forming eruption, volumetric flow rates up to 6 m^3/s were observed [*Schilling et al.*, 2008]. Assuming a circular conduit with diameter around 100 m [*Vallance et al.*, 2008], this gives velocities $\sim 10^{-3}$ m/s. Viscosity of dacite at 850°C with 3 wt% dissolved water and 50% solids by volume is approximately 10^6 Pa s [*Whittington et al.*, 2009; *Costa*, 2005; *Caricchi et al.*, 2007]. Therefore, the Reynolds number scales as

$$Re = \frac{\rho D v}{\eta} \sim \frac{10^3 \, 10^2 \, 10^{-3}}{10^6} \sim 10^{-4},$$ (S1)

where ρ is the density, D is the conduit diameter , v is the velocity and η is the magma viscosity. Since the Reynolds number is very small, we can assume that flow is laminar. The Reynolds number is so small that even for reasonable variations of velocity ($10^{-5} - 10^{-1}$ m/s), conduit diameter ($10^1 - 10^2$ m) and magma viscosity ($10^5 - 10^{10}$ Pa s in the viscous flow regime), the flow would still qualify as laminar. The maximum Reynolds number from this range of values is 10^{-1}.

Second, the Mach number is the flow speed relative to the sound speed in a mixture, where a small value (< 0.3) allows momentum balance to be approximated by the incompressible form, even if $\partial \rho / \partial t$ is not zero. The speed of sound is given by $\sqrt{\partial p / \partial \rho}$ [e.g. *Kundu et al.*, 2012, page 730]. In the nominal model where $v \sim 10^{-3}$ m/s, the minimum sound speed is 70 m/s, giving a Mach number of $\sim 10^{-5}$, very much below the threshold for incompressible flow. For the upper limit of velocities ($\sim 10^{-1}$ m/s), the Mach number is 10^{-2}, thus the incompressible assumption remains valid.

Third, the entrance length determines if flow is fully-developed in the pipe. For laminar flow, the entrance length for the maximum Reynolds number of 10^{-1} scales as [e.g. *Kundu et al.*, 2012, page 803],

$$\frac{l_{\text{entr}}}{D} = 0.06 \, Re \sim 6 \times 10^{-3}.$$ (S2)

For a conduit diameter of 100 m, the entrance length is 0.6 m, small relative to the length of the conduit (nominal value is 4 km) and thus the flow can be assumed to be fully-developed.

Fourth, the cylindrical pipe as applied to a volcanic conduit is assumed to be thin: its radius is much smaller than its length,

$$\epsilon = \frac{R}{L} \sim \frac{10^1}{10^3} \sim 10^{-2}.$$ (S3)

S1.2 Scaling analysis of the Navier-Stokes equation

The general form of the incompressible Navier-Stokes Equation for flow in a vertical cylindrical pipe is given by

$$\frac{\partial v_z}{\partial t} + (\mathbf{v} \cdot \nabla)v_z = -\frac{1}{\rho}\frac{\partial p}{\partial z} - g + \frac{\eta}{\rho}\nabla^2 v_z, \tag{S4}$$

where $\mathbf{v}$ is the velocity field in cylindrical coordinates, v_z is vertical velocity, ρ is magma density, p is pressure, g is gravitational acceleration, η is the fluid shear viscosity, and t, z are the time and vertical space coordinates. Low Mach number justifies the incompressible form of momentum balance. Since flow is fully-developed and laminar (i.e. no turbulent effects), velocities in the radial and tangential directions are zero. Therefore, the only non-zero component of the velocity field is in the vertical direction, $v_z(r, z, t)$, where r is the radial coordinate. These assumptions allow us to eliminate many terms in the expansion of the flux (second term) and Laplacian of velocity (fifth term) in equation S4,

$$(\mathbf{v} \cdot \nabla)v_z = v_r\frac{\partial v_z}{\partial r} + \frac{v_\theta}{r}\frac{\partial v_z}{\partial \theta} + v_z\frac{\partial v_z}{\partial z} \qquad = v_z\frac{\partial v_z}{\partial z} \tag{S5}$$

$$\nabla^2 v_z = \frac{1}{r}\frac{\partial}{\partial r}\left(r\frac{\partial v_z}{\partial r}\right) + \frac{1}{r^2}\frac{\partial^2 v_z}{\partial \theta^2} + \frac{\partial^2 v_z}{\partial z^2} \quad = \frac{1}{r}\frac{\partial}{\partial r}\left(r\frac{\partial v_z}{\partial r}\right) + \frac{\partial^2 v_z}{\partial z^2} \tag{S6}$$

Next, we assign scales (upper case letters) to the equation variables to derive their non-dimensional forms (letters with asterisks),

$$v_z = \mathcal{V}v_z^*, \quad z = \mathcal{L}z^*, \quad r = \mathcal{R}r^*, \quad p = \mathcal{P}p^*, \quad t = \mathcal{T}t^*. \tag{S7}$$

We take $\mathcal{V}$ as a representative velocity in the Mount St. Helens eruption ($\sim 10^{-3}$ m/s), $\mathcal{L}$ as the conduit length ($\sim 10^3$ m), $\mathcal{R}$ as the conduit radius ($\sim 10^1$ m) and $\mathcal{P}$ as the chamber pressure scale ($\sim 10^8$ Pa). An appropriate timescale for $\mathcal{T} \sim \mathcal{L}/\mathcal{V}$. We then replace the variables in the Navier-Stokes equation with their non-dimensional forms,

$$\frac{\mathcal{V}}{\mathcal{T}}\frac{\partial v_z^*}{\partial t^*} + \frac{\mathcal{V}^2}{\mathcal{L}}v_z^*\frac{\partial v_z^*}{\partial z^*} = -\frac{\mathcal{P}}{\mathcal{L}}\frac{1}{\rho}\frac{\partial p^*}{\partial z^*} - g + \frac{\eta}{\rho}\left[\frac{\mathcal{V}}{\mathcal{R}^2}\frac{1}{r^*}\frac{\partial}{\partial r^*}\left(r^*\frac{\partial v_z^*}{\partial r^*}\right) + \frac{\mathcal{V}}{\mathcal{L}^2}\frac{\partial^2 v_z^*}{\partial z^{*2}}\right]$$

$$= -\frac{\mathcal{P}}{\mathcal{L}}\frac{1}{\rho}\frac{\partial p^*}{\partial z^*} - g + \frac{\eta}{\rho}\frac{\mathcal{V}}{\mathcal{R}^2}\left[\frac{1}{r^*}\frac{\partial}{\partial r^*}\left(r^*\frac{\partial v_z^*}{\partial r^*}\right) + \left(\frac{\mathcal{R}}{\mathcal{L}}\right)^2\frac{\partial^2 v_z^*}{\partial z^{*2}}\right] \tag{S8}$$

Comparing the viscous terms (in square brackets), we can neglect $\partial^2 v_z^*/\partial z^{*2}$ since $\mathcal{R}/\mathcal{L} \ll 1$ (equation S3). Multiplying the resulting equation by $\rho\mathcal{R}^2/(\eta\mathcal{V})$ and substituting $\mathcal{T}$,

$$\frac{\rho\mathcal{R}\mathcal{V}}{\eta}\frac{\mathcal{R}}{\mathcal{L}}\left[\frac{\partial v_z^*}{\partial t^*} + v_z^*\frac{\partial v_z^*}{\partial z^*}\right] = -\frac{\mathcal{P}\mathcal{R}^2}{\eta\mathcal{V}\mathcal{L}}\frac{\partial p^*}{\partial z^*} - \frac{\rho\mathcal{R}^2}{\eta\mathcal{V}}g + \frac{1}{r^*}\frac{\partial}{\partial r^*}\left(r^*\frac{\partial v_z^*}{\partial r^*}\right). \tag{S9}$$

The resulting scale of the left hand side terms is equivalent to the product of the Reynolds number and the conduit radius-to-length ratio. We compare the scale of each

term at two viscosity limits relevant to dome-forming eruptions (Table 1). Deep in the conduit, where viscosity is lower, the pressure gradient balances the gravitational term. The viscous term is negligible in this region. Just below the plug, where viscosity is high, the pressure gradient, gravity and viscous terms are of similar magnitudes and contribute to momentum balance. In both cases, the inertial terms are vanishingly small. As the eruption proceeds and velocity decreases, the inertial scales become even smaller because the velocity is in the numerator. In contrast, the pressure gradient and gravity terms become larger because the velocity is in the denominator.

Table 1.   Scale of each term in the equation S9 for the nominal parameter model.

Location	Viscosity η	Inertial terms $\frac{\rho \mathcal{R} \mathcal{V}}{\eta} \frac{\mathcal{R}}{\mathcal{L}}$	Pressure gradient $\frac{\mathcal{P} \mathcal{R}^2}{\eta \mathcal{V} \mathcal{L}}$	Gravity $\frac{\rho \mathcal{R}^2}{\eta \mathcal{V}} g$	Viscous term 1
Conduit base	10^5	10^{-6}	10^5	10^4	10^0
Just below plug	10^{10}	10^{-11}	10^0	10^{-1}	10^0

The scaling analysis shows that inertial terms can be neglected, thus reducing the momentum balance to

$$0 = -\frac{1}{\rho} \frac{\partial p}{\partial z} - g + \frac{\eta}{\rho} \frac{1}{r} \frac{\partial}{\partial r} \left(r \frac{\partial v_z}{\partial r} \right). \tag{S10}$$

This is the steady, laminar Poiseuille flow equation, which has known solutions for velocity in the pipe [e.g. *Kundu et al.*, 2012, page 315],

$$v_z(r) = \frac{r^2 - R^2}{4\eta} \left(\frac{\partial p}{\partial z} + \rho g \right). \tag{S11}$$

For the 1D conduit model, we average velocity over the conduit area

$$v_{\text{visc}} = \frac{1}{\pi R^2} \int_0^R v_z(r) 2\pi r \, dr = -\frac{R^2}{8\eta} \left(\frac{\partial p}{\partial z} + \rho g \right). \tag{S12}$$

S1.3 Frictional sliding velocity

In Poiseuille flow, pipe walls are often assumed to be no-slip boundaries, i.e. $v(r = R) = 0$ [e.g. *Kundu et al.*, 2012, page 315]. In our model, we instead allow non-zero velocity at the boundary due to frictional slip, obeying the rate-and-state friction law [*Dieterich*, 1979; *Ruina*, 1983]. Due to the low velocities considered in the model, we opt for

the regularized form of rate-and-state friction which is well-behaved as v approaches 0,

$$\frac{\tau_R}{\sigma_c} = f = a \ \text{arcsinh} \left[\frac{v_{\text{fric}}}{2v_r} \exp \left(\frac{f_0 + b \log(\theta/\theta_r)}{a} \right) \right], \tag{S13}$$

where τ_R is the shear stress, σ_c is the effective normal stress (difference between litho-static normal stress and hydrostatic pore pressure), and f is the coefficient of friction. Describing f at a particular sliding velocity v_{fric} and state θ requires a known coefficient of friction f_0 at a reference velocity v_r and reference state θ_r, as well as the rate-dependence a and the state-dependence b. We fix $v_r = 10^{-5}$ m/s and leave f_0 and a as poorly-known parameters in the model. For simplicity, we set $b = 0$, since high temperature sliding experiments of granite indicate that b may not be statistically different from zero [*Blanpied et al.*, 1998]. A consequence of this assumption is that friction is always rate-strengthening.

Combining the viscous and frictional components gives the total magma velocity in the conduit,

$$v = v_{\text{visc}} + v_{\text{fric}} = \frac{\tau_R R}{4\eta} + 2v_r \left[\exp \left(-\frac{f_0}{a} \right) \right] \sinh \left(\frac{\tau_R}{a\sigma_c} \right), \tag{S14}$$

where τ_R is the shear stress along the conduit walls,

$$\tau_R = -\frac{R}{2} \left(\frac{\partial p}{\partial z} + \rho g \right). \tag{S15}$$

S2 Code verification by the method of manufactured solutions

We employ the method of manufactured solutions (MMS) to verify the numerical code without requiring a closed-form analytical solution [see *Salari and Knupp*, 2000]. Verification checks that the numerical code is implemented correctly, but does not imply that the code mimics reality (validation). With respect to our numerical model, MMS verifies that the semi-discretization in depth and numerical differentiation employed by `ode15s` for time integration are implemented correctly and consistently. In this section, we briefly describe the MMS procedure, then present an example for the conduit model.

First, analytical expressions for the field variables $\tilde{y}(z,t)$ are selected as the "manufactured solution". The manufactured solution should be smooth, should satisfy the true boundary conditions and should be differentiable up to the order required by the problem. In the conduit model, the second order depth derivative of pressure arises from vertical gas escape, thus pressure in the manufactured solution should be second-order differentiable.

Second, derivatives of the manufactured solution are analytically evaluated and substituted into the governing equations. However, since the manufactured solution is not the exact solution, the governing equations will not be exactly satisfied, producing an analytical correction term $S(t, \tilde{y})$. The manufactured solution is now the exact solution to the modified system of equations,

$$M(t, \tilde{y}) \frac{\partial \tilde{y}}{\partial t} = F(t, \tilde{y}) + S(t, \tilde{y}). \tag{S16}$$

Third, the numerical code is used to solve the modified system of equations with $S(t, \tilde{y})$ included. When the numerical code is implemented correctly, solving this modified system numerically should reproduce the analytical manufactured solution.

With MMS, we can verify the most complex forms of the conduit model for the present application (with variable viscosity, significant contribution from transient terms, etc.). However, since this method does not easily accommodate abrupt changes in the equations, we leave out the percolation threshold and plug gas loss and instead verify these equation switches by comparing results to steady-state solutions.

S2.1 Example manufactured solution

We tested different manufactured solutions and here present an example where field variables vary exponentially in depth and sinusoidally in time, both of which are infinitely differentiable. For example, the manufactured pressure field is

$$\tilde{p}(z,t) = p_{\text{top}} \exp\left(-\frac{z}{L} \ln \frac{p_{\text{ch}}(t)}{p_{\text{top}}}\right), \quad \text{where } p_{\text{ch}}(t) = p_{\text{ch}}^0 + \delta p \sin\left(\frac{t}{t_c}\right) \tag{S17}$$

$$\frac{\partial \tilde{p}}{\partial t} = -\tilde{p} \frac{z}{L} \frac{1}{p_{\text{ch}}} \frac{dp_{\text{ch}}}{dt} \tag{S18}$$

$$\frac{\partial \tilde{p}}{\partial z} = -\frac{\tilde{p}}{L} \ln \frac{p_{\text{ch}}(t)}{p_{\text{top}}}. \tag{S19}$$

To describe $p_{\text{ch}}(t)$ in $\tilde{p}(z,t)$, we specify the initial chamber pressure p_{ch}^0, as well as the amplitude δp and period t_c of sinusoidal evolution. By construction, the boundary conditions for pressure at the conduit bottom $\tilde{p}(z = -L, t) = p_{\text{ch}}(t)$ and the top $\tilde{p}(z = 0, t) = p_{\text{top}}$ are satisfied. Similar forms were derived for velocity, porosity and mole fraction of water. These analytical expressions, as well as their respective derivatives, were then substituted into the governing equations to derive the analytical correction term $S(t, \tilde{y})$. Taking the

solids and liquids equation as an example, the correction term would be

$$
\begin{aligned}
S_{sl} &= \frac{\partial}{\partial t}\left(\rho_s \tilde{\phi}_s + \rho_l \tilde{\phi}_l\right) + \frac{\partial}{\partial z}\left(\rho_s \tilde{\phi}_s + \rho_l \tilde{\phi}_l\right) v \\
&= \tilde{M}_p \frac{\partial \tilde{p}}{\partial t} + \tilde{M}_{\phi_g} \frac{\partial \tilde{\phi}_g}{\partial t} + \tilde{M}_{m_h} \frac{\partial \tilde{M}_h}{\partial t} + v\left(\tilde{M}_p \frac{\partial \tilde{p}}{\partial z} + \tilde{M}_{\phi_g} \frac{\partial \tilde{\phi}_g}{\partial z} + \tilde{M}_{m_h} \frac{\partial \tilde{M}_h}{\partial z}\right) + \left(\rho_s \tilde{\phi}_s + \rho_l \tilde{\phi}_l\right) \frac{\partial \tilde{v}}{\partial z},
\end{aligned}
$$

(S20)

where tildes indicate dependent variables evaluated from the manufactured solution. For example, $\tilde{M}_j = \partial\left(\rho_s \tilde{\phi}_s + \rho_l \tilde{\phi}_l\right)/\partial \tilde{j}$, where $j = p, \phi_g, m_h$, which has already been analytically evaluated when deriving the mass matrix $M(t, y)$ for the governing equations, and simply requires substitution with the manufactured field variables and derivatives. Both time and depth derivatives in the above equation are in analytical form (e.g. equations S18, S19). In contrast, in the numerical scheme, the depth derivative is estimated using finite differences, while time derivative is estimated using the numerical differentiation formulas employed by `ode15s`.

The same approach is used to derive the analytical correction term for the volatile continuity equations and the momentum balance. Analytical expressions of the correction term is then written into the function that evaluates the right side of the governing equations (equation S16), and the modified system of equations is time-stepped using `ode15s`.

Comparing the numerical solution (red crosses) with the manufactured solution (blue line) shows good agreement in both time and depth (Figure S1). To ensure convergence of the numerical solution, we tested different depth discretizations using the same parameters (Figure S2). Errors were derived from the difference of the solutions at the simulation end time and normalized by the manufactured solution. Both the 2-norm error and the maximum error show convergence to the manufactured solution. The 2-norm error converges between 2nd and 3rd order, while the maximum error converges at 3rd order, consistent with our spatial discretization schemes: central difference, used to estimate pressure gradient, is 2nd order accurate, while QUICK, used to interpolate cell face values, is 3rd order accurate [*Leonard*, 1995].
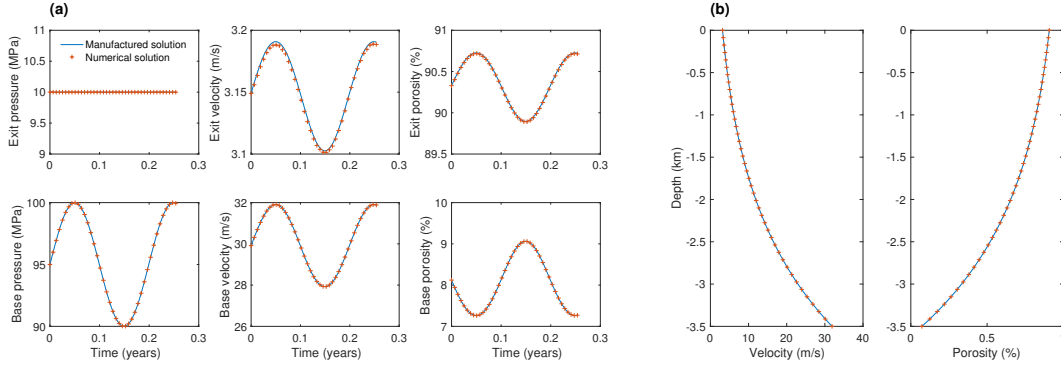
Figure S1. Comparison of numerical solution (red crosses) with manufactured solution (blue line): (a) Temporal evolution of pressure, velocity and porosity at conduit top (top row) and base (bottom row). (b) Depth profiles of velocity and porosity at simulation end time. Model parameters: initial chamber pressure $p_{ch0} = 95$ MPa at depth 3.5 km, sinusoidal pressure evolution with amplitude $\delta p = 5$ MPa and period $t_c = 0.2$ years, $R = 80$ m, $k_c = 10^{-13}$ m^2, $f_0 = 0.2$, $\chi_h^{ch} = 5$ wt%, $\chi_c^{ch} = 1000$ ppm.
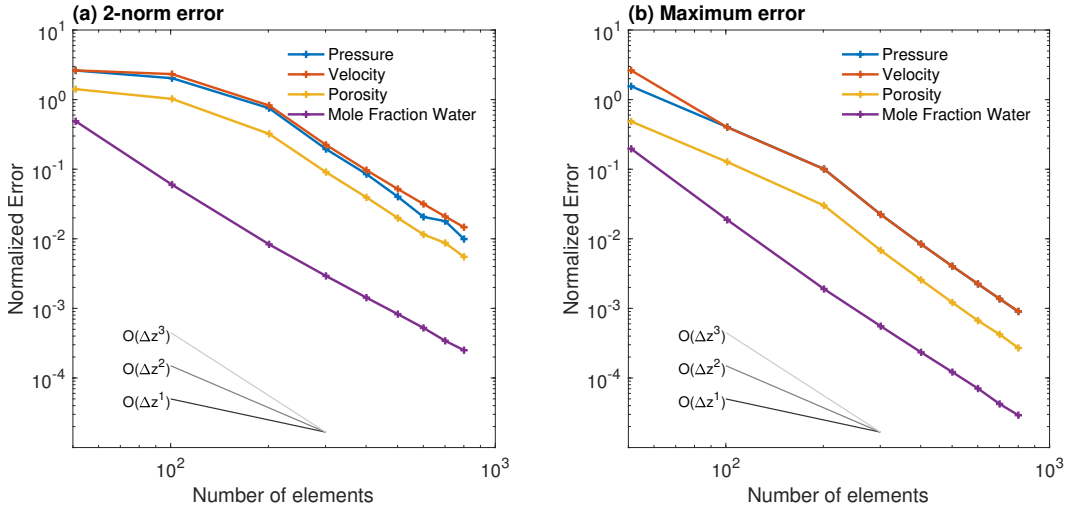

Figure S2. Convergence test of numerical solution compared to manufactured solution, with model parameters as in Figure S1: (a) 2-norm error, while (b) maximum error (infinity norm), both normalized by the manufactured solution. For comparison, the gray lines show, in increasing order of steepness, convergence rates at 1st, 2nd and 3rd order.

S3 Distance-based Generalized Sensitivity Analysis

We employ the Distance-based Generalized Sensitivity Analysis (DGSA) to examine the influence of model parameters on predicted time-series data of 1100 randomly-sampled model realizations [*Fenwick et al.*, 2014]. These 1100 samples span a wide range of T_{ch}/T_{asc}, with most models under 1000 (Figure S3).

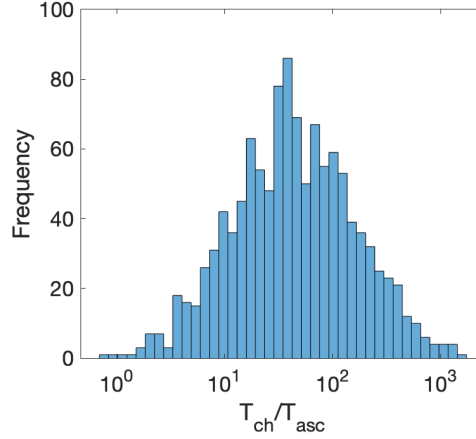**Figure S3.** Distribution of T_{ch}/T_{asc} for the 1100 model realizations used for DGSA.

We describe the intermediate steps of DGSA using the example of the full and normalized time series of extruded volume. First, DGSA separates the predicted extruded volume time series into different classes using k-medoids clustering [*Kaufman and Rousseeuw*, 1990]. Here, we choose to use 4 classes. No appreciable difference in the sensitivity rankings was derived for a larger number of classes. For the full time series, the model predictions are classified based mainly on the total volume at the simulation end time (Figure S4a), while in the normalized time series, the responses are classified based on their temporal evolution (Figure S4b).

Second, DGSA derives the empirical cumulative distribution functions (CDFs) of the model parameters within each class (called the "class-conditional empirical distribution") (Figure S5). Each class-conditional empirical distribution is compared with the empirical distribution of the whole sample set (called the "prior empirical distribution", here approximately a uniform distribution). If the extruded volume time series is sensitive to a parameter, each class will contain a distinctive distribution of the parameter. For example, classes with larger extruded volumes tend to have a greater proportion of large conduit
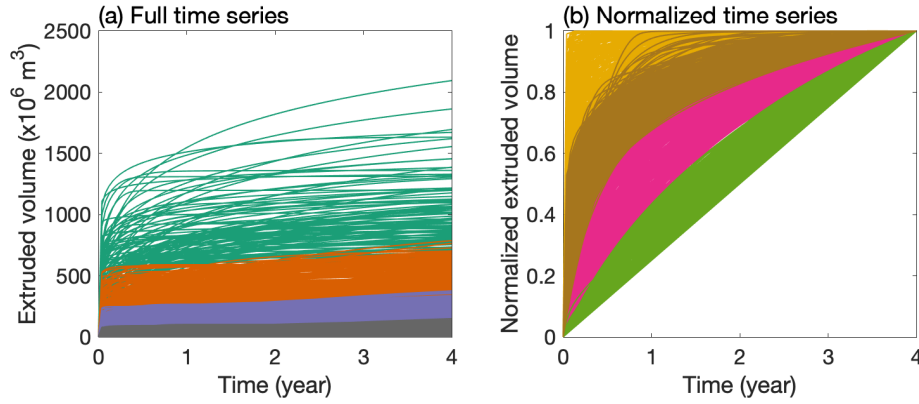
Figure S4. Classification of predicted extruded volume: (a) full time series, (b) normalized time series. Different colors indicate different classes.

radii (green lines in Figures S4a, S5a). Otherwise, the distributions will resemble one another (e.g. magma permeability scale in Figure S5a). Parameters that are slightly sensitive will show modest deviations from the prior distribution (e.g. magma permeability scale in Figure S5b).

Third, DGSA calculates the distances between the prior CDF and each class-conditional CDF to derive the parameter sensitivity for each class (here called the Standardized Sensitivity to maintain consistent terminology with *Fenwick et al.* [2014]; *Park et al.* [2016]) (Figure S6). If the sensitivity is greater than 1 in any of the classes, the model predictions are deemed to be sensitive to that parameter.

Finally, the sensitivities for each parameter are averaged over all the classes to derive Figure 10 in the main text.
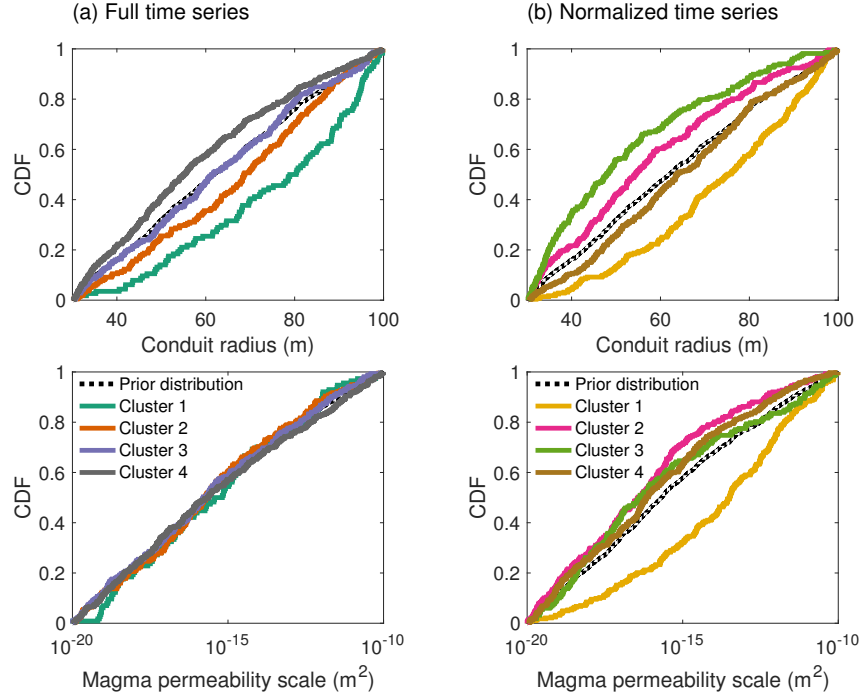
Figure S5. Class-conditional empirical cumulative distribution functions (CDFs) of radius and magma permeability scale within each class for (a) the full time series and (b) the normalized time series of the predicted extruded volume. Colors correspond to Figure S4. In all plots, black dashed line represents the prior empirical CDF for the whole set of model realizations.
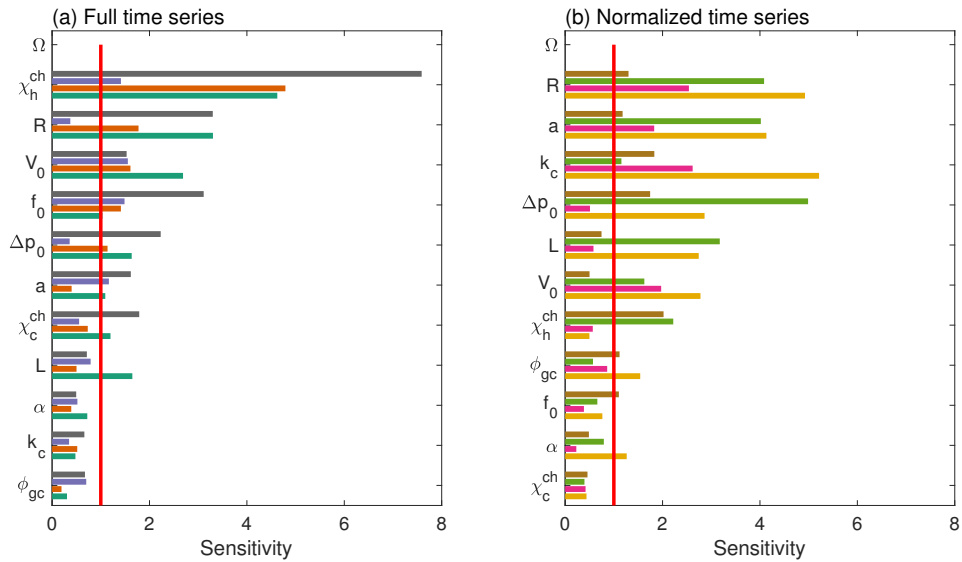

Figure S6. Sensitivity measured for each class for the (a) full time series and (b) normalized time series of the predicted extruded volume. Each model parameter has four bars representing four classes of predicted extrusion volume. Colors correspond to Figures S4 and S5.

References

Blanpied, M. L., C. J. Marone, D. a. Lockner, J. D. Byerlee, and D. P. King (1998), Quantitative measure of the variation in fault rheology due to fluid-rock interactions, *Journal of Geophysical Research*, *103*(98), 9691, doi:10.1029/98JB00162.

Caricchi, L., L. Burlini, P. Ulmer, T. Gerya, M. Vassalli, and P. Papale (2007), Non-Newtonian rheology of crystal-bearing magmas and implications for magma ascent dynamics, *Earth and Planetary Science Letters*, *264*(3-4), 402–419, doi:10.1016/j.epsl.2007.09.032.

Costa, A. (2005), Viscosity of high crystal content melts: Dependence on solid fraction, *Geophysical Research Letters*, *32*(22), 1–5, doi:10.1029/2005GL024303.

Dieterich, J. H. (1979), Modeling of rock friction 1. Experimental results and constitutive equations, *Journal of Geophysical Research: Solid Earth*, *84*(B5), 2161–2168, doi:10.1029/JB084iB05p02161.

Fenwick, D., C. Scheidt, and J. Caers (2014), Quantifying Asymmetric Parameter Interactions in Sensitivity Analysis: Application to Reservoir Modeling, *Mathematical Geosciences*, *46*(4), 493–511, doi:10.1007/s11004-014-9530-5.

Kaufman, L., and P. J. Rousseeuw (1990), Partitioning around medoids (program pam), in *Finding Groups in Data: An Introduction to Cluster Analysis*, pp. 68–125, Wiley, New York.

Kundu, P. K., I. M. Cohen, and D. R. Dowling (2012), *Fluid Mechanics*, 5th ed., Elsevier Inc.

Leonard, B. P. (1995), Order of accuracy of QUICK and related convection-diffusion schemes, *Applied Mathematical Modelling*, *19*(11), 640–653, doi:10.1016/0307-904X(95)00084-W.

Park, J., G. Yang, A. Satija, C. Scheidt, and J. Caers (2016), DGSA: A Matlab toolbox for distance-based generalized sensitivity analysis of geoscientific computer experiments, *Computers and Geosciences*, *97*, 15–29, doi:10.1016/j.cageo.2016.08.021.

Ruina, A. (1983), Slip instability and state variable friction laws, *Journal of Geophysical Research*, *88*, 10,359, doi:10.1029/JB088iB12p10359.

Salari, K., and P. Knupp (2000), Code Verification by the Method of Manufactured Solutions, *Tech. rep.*, Sandia National Laboratories, Albuquerque, New Mexico.

Schilling, S. P., R. Thompson, J. Messerich, and E. Y. Iwatsubo (2008), Use of Digital
Aerophotogrammetry to Determine Rates of Lava Dome Growth, Mount St. Helens,
Washington, 2004-2005, *A Volcano Rekindled: The Renewed Eruption of Mount St. He-
lens 2004-2006, U.S. Geological Survey Professional Paper 1750*, pp. 145–167.

Vallance, J., D. Schneider, and S. Schilling (2008), Growth of the 2004-2006 Lava-Dome
Complex at Mount St. Helens, Washington, *A Volcano Rekindled: The Renewed Erup-
tion of Mount St. Helens 2004-2006, U.S. Geological Survey Professional Paper 1750*, pp.
169–208.

Whittington, A. G., B. M. Hellwig, H. Behrens, B. Joachim, A. Stechern, and F. Vetere
(2009), The viscosity of hydrous dacitic liquids: Implications for the rheology of evolv-
ing silicic magmas, *Bulletin of Volcanology*, *71*(2), 185–199, doi:10.1007/s00445-008-
0217-y.